J. Fluid Mech. (2009), *vol.* 640, *pp.* 55–77. © Cambridge University Press 2009
doi:10.1017/S002211200999156X

Streaming potential generated by a drop moving along the centreline of a capillary

ETIENNE LAC[1]† AND J. D. SHERWOOD[2]

[1]Schlumberger Doll Research, One Hampshire Street, Cambridge MA 02139-1578, USA

[2]Department of Applied Mathematics and Theoretical Physics, University of Cambridge, Wilberforce Road, Cambridge CB3 0WA, UK.

(Received 30 May 2008; revised 5 August 2009; accepted 12 August 2009; first published online 12 November 2009)

The electrical streaming potential generated by a two-phase pressure-driven Stokes flow in a cylindrical capillary is computed numerically. The potential difference $\Delta\Phi$ between the two ends of the capillary, proportional to the pressure difference Δp for single-phase flow, is modified by the presence of a suspended drop on the centreline of the capillary. We determine the change in $\Delta\Phi$ caused by the presence of an uncharged insulating neutrally buoyant drop at a small electric Hartmann number, i.e. when the perturbation to the flow field caused by electric stresses is negligible.

The drop velocity and deformation, and the consequent changes in the pressure difference Δp and streaming potential $\Delta\Phi$, depend upon three independent parameters: the size a of the undeformed drop relative to the radius R of the capillary; the viscosity ratio λ between the drop phase and the continuous phase; and the capillary number Ca which measures the ratio of viscous to capillary forces. We investigate how the streaming potential depends on these parameters: purely hydrodynamic aspects of the problem are discussed by Lac & Sherwood (*J. Fluid Mech.*, doi:10.1017/S0022112009991212).

The potential on the capillary wall is assumed sufficiently small so that the electrical double layer is described by the linearized Poisson–Boltzmann equation. The Debye length characterizing the thickness of the charge cloud is taken to be small compared with all other length scales, including the width of the gap between the drop and the capillary wall. The electric potential satisfies Laplace's equation, which we solve by means of a boundary integral method. The presence of the drop increases $|\Delta\Phi|$ when the drop is more viscous than the surrounding fluid ($\lambda > 1$), though the change in $|\Delta\Phi|$ can take either sign for $\lambda < 1$. However, the difference between $\Delta\Phi$ and Δp (suitably non-dimensionalized) is always positive. Asymptotic predictions for the streaming potential in the case of a vanishingly small spherical droplet, and for large drops at high capillary numbers, agree well with computations.

1. Introduction

Streaming potentials are generated when fluid flows past a charged surface. Convection of electric charges within the charge cloud adjacent to the surface leads to a current; if there is no external return path for the current, a potential is established and current returns via conduction through the fluid. The phenomenon is well understood for single-phase flows, for which there is a linear relationship

† Email address for correspondence: elac@slb.com

https://doi.org/10.1017/S002211200999156X Published online by Cambridge University Press

between the pressure drop that drives the flow and the electrical potential difference generated by fluid motion. However, much less is known about streaming potentials generated by multiphase flow (Morgan, Williams & Madden 1989; Antraygues & Aubert 1993; Sprunt, Mercer & Djabbarah 1994; Guichet, Jouniaux & Pozzi 2003; Revil & Cerepi 2004; Jackson 2008). Such flows are of importance in soil, in which the pore space is filled by an air–water mixture, and in petroleum reservoirs (saturated by oil–water–gas mixtures). Potential practical applications include the detection of water approaching a production well (Wurmstich & Morgan 1994; Jackson, Saunders & Addiego-Guevara 2005; Saunders, Jackson & Pain 2006, 2008) and the generation of electrokinetic signals as seismic waves pass a gas–liquid interface.

Previous theoretical analysis of the streaming potential generated by a bubble or drop flowing in a fluid-filled capillary has considered a closely fitting sphere (rigid or inviscid) or a Bretherton bubble (Sherwood 2007, 2008). Here we compute the streaming potential generated as a drop of viscosity $\lambda\mu$ moves along the centreline of a capillary filled by a second fluid of viscosity μ. This represents an idealized two-phase flow in a porous medium: the geometry of a realistic porous material (e.g. rock) is much more complex. The presence of the drop is known to modify the pressure difference necessary to maintain a given flow rate or, equivalently, the flow rate driven by a constant pressure difference (Olbricht 1996). We similarly expect the drop to affect the streaming potential generated between the ends of the capillary, since both the convective current in the electric double layer and the overall electrical resistance of the capillary are modified by the presence of the drop. Our main objective is to quantify the influence of a dispersed phase on the relationship between the pressure drop and the streaming potential. For the sake of simplicity, we shall consider the case of a perfectly insulating drop, so that electric currents are present only in the bulk of the suspending liquid. The ζ-potential at the surface of the capillary wall is assumed to be small and uniform, and the surface of the drop is uncharged. The charge cloud at the wall of the capillary is assumed to be thin compared to the radius R of the capillary and to the width h of the gap between the drop and the capillary wall. In consequence, electric Hartmann numbers are small: the electric potential induced by the flow generates negligibly small electrohydrodynamic flows compared to the original pressure-driven flow. This simplifying assumption enables us to decouple the hydrodynamics and the electrokinetics. Therefore we first solve the flow field due to the motion of the drop in the capillary assuming creeping flow conditions and determine *a posteriori* the induced streaming potential. We have discussed in detail the hydrodynamic effects in a companion paper (Lac & Sherwood, 2009) and concentrate here on the electrokinetic aspects.

The governing equations for the electrokinetic problem are set down in § 2. Section 3 presents our numerical method for deformable drops of arbitrary size and for spherical drops of infinite surface tension fitting in the tube. We first present asymptotic predictions for small drops (§ 4.1) and for long slender drops (§ 4.2) moving along the centreline of the capillary. Numerical results for drops of arbitrary size follow in § 5. Finally we discuss our results and possible directions for future research in § 6.

2. Governing equations

2.1. *Hydrodynamics*

We consider the motion of a liquid drop in a cylindrical capillary of radius R filled with another liquid. The drop consists of an incompressible Newtonian liquid of density $\bar{\rho}$, dynamic viscosity $\bar{\mu}$ and volume $\mathscr{V}$; its size is characterized by the radius

https://doi.org/10.1017/S002211200999156X Published online by Cambridge University Press

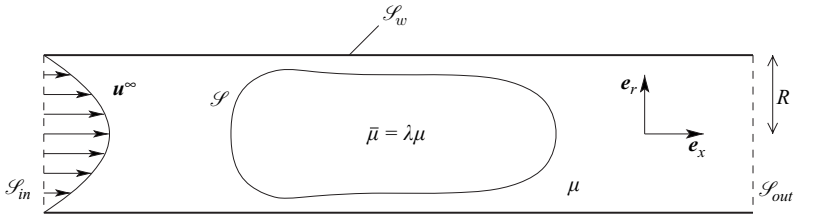


FIGURE 1. Representation of a drop suspended in a pressure-driven flow.

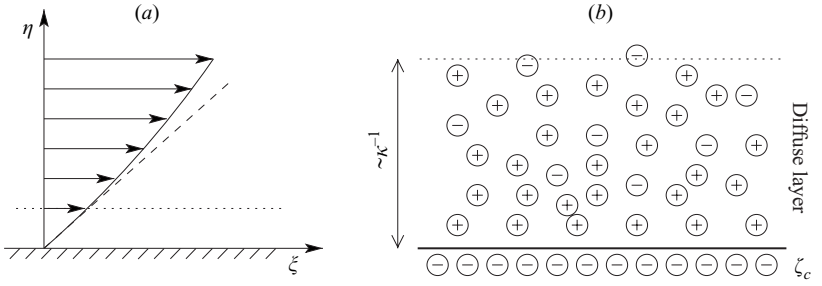


FIGURE 2. Schematic of the origin of a streaming current: a diffuse charge cloud forms in the vicinity of the charged wall, and electric charges are convected by the flow.

a of the sphere of volume $\mathscr{V} = (4/3)\pi a^3$. The suspending liquid has density $\rho = \bar{\rho}$ and dynamic viscosity μ and flows at constant volumetric flow rate $\pi R^2 U$ under the action of a pressure gradient G along the capillary. The coefficient of interfacial tension between the two phases is denoted by γ. In the absence of the drop, the (single-phase) flow reduces to a Poiseuille flow, with

$$U = -\frac{R^2 G_0}{8\mu}, \tag{2.1}$$

where G_0 is the (uniform) pressure gradient.

The boundaries of the domain are the entrance and exit sections $\mathscr{S}_{in}$ and $\mathscr{S}_{out}$, the solid surface of the capillary $\mathscr{S}_w$ and the drop/medium interface $\mathscr{S}$, as depicted in figure 1. Note that hereafter, barred variables refer to the drop phase.

The Reynolds number $Re = \rho R U/\mu$ is usually small in flow through low-permeability materials, and we neglect inertia in the equations of fluid motion. Far behind and ahead of the drop, the outer flow reduces to a Poiseuille flow, since the flow perturbation generated by a point-force distribution in a Stokes flow decays exponentially downstream and upstream (Liron & Shahar 1978). The solution of the Stokes equations by means of boundary integrals has been discussed in detail by Martinez & Udell (1990), Tsai & Miksis (1994) and Lac & Sherwood (2009).

2.2. *Streaming potential due to a ζ-potential on the capillary wall*

We assume that the capillary wall is electrically charged, with a uniform ζ-potential ζ_c. Counter-ions in the suspension liquid accumulate in a thin cloud at the vicinity of the wall, as depicted in figure 2. The charge in the cloud is equal to and opposite that on the wall, so that the double layer (cloud + wall) is electrically neutral. The thickness of the diffuse charge cloud is characterized by the Debye length κ^{-1}. Assuming this length is negligibly small compared to the other length scales of the problem, we may use a plane approximation to describe the electric double layer.

https://doi.org/10.1017/S002211200999156X Published online by Cambridge University Press

We consider a charged plane wall with local coordinates (ξ, η), where η measures the distance normal from the wall (figure 2*a*). As the liquid moves past the wall, it entrains the electric charges of the diffuse layer, which creates a streaming current (per unit length in the vorticity direction)

$$\boldsymbol{j}_c = \int_0^\infty \rho_e \boldsymbol{u}\, \mathrm{d}\eta, \tag{2.2}$$

where ρ_e denotes the excess charge density in the diffuse charge cloud adjacent to the wall. Owing to the negligible thickness of the diffuse layer, the velocity field in the charged region may be approximated by

$$\boldsymbol{u} \approx \eta \left(\frac{\partial \boldsymbol{u}}{\partial \eta}\right)_w = \eta \left(\frac{\partial u_\xi}{\partial \eta}\right)_w \boldsymbol{e}_\xi, \tag{2.3}$$

where $\boldsymbol{e}_\xi$ is the unit vector in the direction ξ and $u_\xi = \boldsymbol{u}\cdot\boldsymbol{e}_\xi$. We assume $\zeta_c \ll kT/e$, where $-e$ is the electronic charge and kT is the Boltzmann temperature, so that the Poisson–Boltzmann equation describing the equilibrium charge cloud may be linearized. It may then be shown (Hunter 1981) that

$$\rho_e \approx -\varepsilon \kappa^2 \zeta_c \, \mathrm{e}^{-\kappa\eta}. \tag{2.4}$$

Including (2.3) and (2.4) in (2.2) yields the approximation

$$\boldsymbol{j}_c \approx -\varepsilon\, \zeta_c \left(\frac{\partial u_\xi}{\partial \eta}\right)_w \boldsymbol{e}_\xi. \tag{2.5}$$

If there is no return path for the electric current other than the pore itself, the convective current has to be balanced by a counter-current in the bulk, driven by an electric field $\boldsymbol{E}$. At steady state, the electric field may be written as $\boldsymbol{E} = -\nabla\Phi$, such that

$$\nabla\cdot\boldsymbol{E} = -\nabla^2\Phi = 0, \tag{2.6}$$

where Φ is the electric potential, referred to as the 'streaming potential'.

In the case of a single-phase pressure-driven flow in a cylindrical tube with no external return path for the electric current, the streaming electric field has to satisfy

$$2\pi R\, \boldsymbol{j}_c + \pi R^2 \sigma \boldsymbol{E} = 0, \tag{2.7}$$

where σ denotes the bulk conductivity of the fluid and where any surface conductivity along the capillary wall has been neglected. Note that with the cylindrical coordinates (x, r, φ) such that $\boldsymbol{e}_x$ is aligned with the tube axis (figure 1), $\boldsymbol{e}_x = \boldsymbol{e}_\xi$ and $\boldsymbol{e}_r = -\boldsymbol{e}_\eta$. The wall shear rate $4U/R = -RG_0/(2\mu)$ is uniform, so that (2.5) yields $\boldsymbol{j}_c = -4(\varepsilon\zeta_c U/R)\,\boldsymbol{e}_x$, and hence, by (2.7), $\boldsymbol{E} = E\,\boldsymbol{e}_x = 8\varepsilon\zeta_c U/(\sigma R^2)\,\boldsymbol{e}_x$. Alternatively, we may express the mean velocity U as a function of the pressure gradient G_0 and write

$$E = -\frac{\varepsilon\,\zeta_c}{\sigma\mu} G_0, \quad \text{i.e.} \quad \left(\frac{\sigma R^2}{\varepsilon\zeta_c U}\right)\frac{\partial\Phi}{\partial x} = \left(\frac{R^2}{\mu U}\right)\frac{\partial p}{\partial x}. \tag{2.8}$$

If lengths are scaled by R, stresses by $\mu U/R$ and electric fields by $\varepsilon\zeta_c U/\sigma R^2$, (2.8) shows that the dimensionless electric potential is equal to the dimensionless pressure (to within an arbitrary constant). The ratio $-\sigma E/G_0 = \varepsilon\,\zeta_c/\mu = K$ is often referred to as the 'coupling parameter'.

Our neglect of the surface conductivity due to the mobile charge cloud at the capillary wall is easy to justify when $e|\zeta_c|/(kT) \ll 1$ (e.g. Sherwood 2007). In rock there may also be significant surface conductivity within the Stern layer of ions adsorbed at

https://doi.org/10.1017/S002211200999156X Published online by Cambridge University Press

the capillary wall (Revil *et al.* 1999). The effect of such surface conductivity has been considered by Sherwood (2007, 2008) and may be important if the film between the drop and capillary wall is thin. However, at the higher capillary numbers considered here, the film of fluid around the drop is sufficiently thick so that its electrical conductance is large, and surface conductivity can usually be neglected.

The analysis leading to the charge density (2.4) assumes point charges, with no restriction on the ionic number densities. In practice, when ion densities are high and Debye lengths κ^{-1} small, there may be insufficient space for the ions, and the equilibrium charge cloud is poorly represented by (2.4). However, if ion densities are high, the fluid conductivity σ is large, and streaming potentials will be small; so this limit is of little interest. On the other hand, if ion densities are low, the double-layer thickness κ^{-1} will be larger, and we need to check that κ^{-1} is small compared to the liquid film thickness h.

The presence of the drop disturbs the outer flow and creates a variation of the wall shear rate. Therefore, according to (2.5), the convective current $\boldsymbol{j}_c$ is no longer uniform along the capillary wall. Owing to charge conservation, a local variation of the streaming current must be balanced by a charge flux into or out of the electric double layer. This induces a normal electric field E_n at the wall, given by

$$\nabla_s \cdot \boldsymbol{j}_c = -\sigma E_n = \sigma \frac{\partial \Phi}{\partial n}, \quad \text{where} \quad \frac{\partial \Phi}{\partial n} \equiv \nabla \Phi \cdot \boldsymbol{n}, \tag{2.9}$$

and $\boldsymbol{n}$ is the normal into the fluid (Brunet & Ajdari 2006). We shall assume that the drop is perfectly insulating, implying that on its surface

$$\frac{\partial \Phi}{\partial n}(\boldsymbol{x}) = 0, \qquad \forall \boldsymbol{x} \in \mathscr{S}. \tag{2.10}$$

Since the flow reduces to a Poiseuille flow far away from the drop, the electric field at the entry and exit sections is given by (2.8), which yields a boundary condition for $\partial \Phi / \partial n$ on $\mathscr{S}_{in}$ and $\mathscr{S}_{out}$.

When the capillary contains a long cylindrical insulating drop of radius $R\delta$, the electric field $\boldsymbol{E}$ generated by a pressure gradient G is greater than that estimated in (2.8) by a factor $(1-\delta^2)^{-1}$ and has typical magnitude

$$|\boldsymbol{E}| = \frac{\varepsilon |\zeta_c|}{\sigma \mu} \frac{|G|}{1-\delta^2}. \tag{2.11}$$

This electric field, acting on the charge density ρ_e (2.4) produces a body force $\rho_e \boldsymbol{E}$ which is small compared to the imposed pressure gradient if

$$\frac{He}{1-\delta^2} \ll 1, \tag{2.12}$$

where

$$He = \frac{(\varepsilon \kappa \zeta_c)^2}{\sigma \mu} \tag{2.13}$$

is an electric Hartmann number. In order to estimate the magnitude of He, we first set $\sigma = \varepsilon k T \kappa^2 \omega$, where ω is an average ionic mobility, with $\omega \approx 4 \times 10^{11}\,\mathrm{m\,s^{-1}N^{-1}}$ for an aqueous solution of NaCl. Thus $He = (e\zeta_c/kT)^2 \varepsilon k T/(\mu \omega e^2)$. Taking $T = 300\,\mathrm{K}$ and $\mu = 10^{-3}\,\mathrm{Pa\,s}$ (water), we find the factor $\varepsilon k T/(\mu \omega e^2) \approx 0.28$, and since we have assumed $e|\zeta_c|/(kT) \ll 1$ we conclude that He is always small. The charge cloud is adjacent to the rigid wall of the capillary, and the electric force acting on it perturbs the fluid velocity by an amount $O(R\kappa)^{-1}$ less than predicted by the above arguments

https://doi.org/10.1017/S0022112009991566 Published online by Cambridge University Press

(Sherwood 2008). Setting $1-\delta^2 \approx 2h/R \ll 1$, we conclude that the perturbation to the velocity field is small if $He/(\kappa h) \ll 1$, which always holds if (as assumed here) $\kappa h \gg 1$. However, if we were to consider the effect of the electric field on a charge cloud at the surface of the drop, away from rigid boundaries, a stronger condition $He\,R/h \ll 1$ would have to be satisfied for velocity perturbations to be neglected.

Even in the absence of any charge cloud at the surface of the drop, the electric field generated by fluid motion leads to Maxwell stresses which scale as $\varepsilon|\boldsymbol{E}|^2$ (Melcher & Taylor 1969; Saville 1997). These stresses are largest when $h/R = 1-\delta \ll 1$, i.e. when $|\boldsymbol{E}|$ as given by (2.11) is large. In this limit, the drop, of viscosity $\lambda\mu$, occupies almost the entire cross-section of the capillary. The viscous stress at its surface is approximately $|GR|/2$, where the pressure gradient $G \approx \lambda G_0$ (see § 4.2) and $G_0 = -8\mu U/R^2$ after (2.1). Hence, by (2.11), the Maxwell stresses are small compared to viscous stresses if

$$\varepsilon|\boldsymbol{E}|^2 \sim \varepsilon\left(\frac{\varepsilon\zeta_c}{\sigma\mu}\frac{\lambda\mu U}{hR}\right)^2 \ll \frac{\lambda\mu U}{R}, \qquad \text{i.e.} \qquad \frac{\lambda\, Pe\, He}{\kappa R\,(\kappa h)^2} \ll 1, \tag{2.14}$$

where

$$Pe = \frac{U}{\omega k T \kappa} \tag{2.15}$$

is a Péclet number; Pe is typically small, since $\omega k T \kappa \approx 1.7\,\mathrm{m\,s^{-1}}$ for the conditions discussed above. Condition (2.14) is therefore usually easily satisfied, since $He \ll 1$ and $\kappa R > \kappa h \gg 1$.

Capillary stresses might be either $O(\gamma/a)$ or $O(\gamma/R)$. However, when $a > R$, the drop has to deform to fit within the capillary, so that capillary stresses are at least $\gamma/R = (\mu U/R)\,Ca^{-1}$, where the capillary number $Ca = \mu U/\gamma$ measures the ratio of viscous to interfacial stresses. Maxwell stresses are therefore small compared to capillary stresses if

$$\frac{\lambda^2\, Ca\, Pe\, He}{\kappa R\,(\kappa h)^2} \ll 1. \tag{2.16}$$

The capillary numbers that we shall consider are at most $Ca \approx 3$. We conclude from (2.14) and (2.16) that Maxwell stresses are always negligible.

Thus when $\varepsilon|\zeta_c|/(kT) \ll 1$ and as long as $\kappa h \gg 1$, we can assume that electric stresses are small: the streaming potential is coupled with the hydrodynamics through (2.9) and (2.5) but has a negligible feedback effect on the drop behaviour. As a consequence, we may first solve the flow field described in § 2.1 and determine the induced streaming potential in a post-processing step. Should condition (2.14) or (2.16) fail, electrohydrodynamic phenomena would modify the flow inside and outside the drop: the hydrodynamics and electrokinetics would then have to be be solved simultaneously.

At the capillary wall, the shear rate is proportional to the viscous stress $\boldsymbol{f}^w$, with

$$\mu\left(\frac{\partial \boldsymbol{u}}{\partial n}\right)_w = (\boldsymbol{I}-\boldsymbol{nn})\cdot\boldsymbol{f}^w. \tag{2.17}$$

Using (2.17), we may express the streaming current $\boldsymbol{j}_c$ (2.5) in terms of the viscous stress $\boldsymbol{f}^w$ at the wall and then determine the boundary condition (2.9) for the electric potential Φ at the capillary wall. Applying Green's third identity to the potential Φ and using (2.10), we may finally write, for any point $\boldsymbol{x}$ located on either boundary of

https://doi.org/10.1017/S0022112009991566 Published online by Cambridge University Press

	scaled by
Lengths	R
Velocities	U
Stresses	$\mu U/R$
Electric current densities	$\varepsilon\zeta_c U/R^2$
Streaming potentials	$\dfrac{\varepsilon\zeta_c U}{\sigma R}$

TABLE 1. Summary of the scaling chosen for physical quantities of interest. Non-dimensional quantities are denoted by an asterisk in the text.

the domain,

$$2\pi\,\Phi(\boldsymbol{x}) = \oint_{\partial\Omega} \left\{ \frac{\hat{\boldsymbol{r}}\cdot\boldsymbol{n}}{\hat{r}^3}\,\Phi(\boldsymbol{y}) + \frac{1}{\hat{r}}\frac{\partial\Phi}{\partial n} \right\} \mathrm{d}S(\boldsymbol{y}) + \oint_{\mathscr{S}} \frac{\hat{\boldsymbol{r}}\cdot\boldsymbol{n}}{\hat{r}^3}\,\Phi(\boldsymbol{y})\,\mathrm{d}S(\boldsymbol{y}), \tag{2.18}$$

where $\hat{\boldsymbol{r}} = \boldsymbol{y}-\boldsymbol{x}$; $\hat{r} = |\hat{\boldsymbol{r}}|$; $\partial\Omega \equiv \mathscr{S}_{in} \cup \mathscr{S}_{out} \cup \mathscr{S}_w$; and $\boldsymbol{n}$ is the unit normal vector pointing inward into the suspending liquid. The term $\partial\Phi/\partial n$ is known on every boundary; so the unknown of (2.18) is the electric potential distribution at the wall and at the drop interface, as well as the uniform potentials Φ_{in} and Φ_{out} at the entrance and exit sections. Since Φ is defined only to within an arbitrary constant, we set $\Phi_{in} = 0$. Furthermore, Φ_{out} may be removed from the list of unknowns because it is equal to the wall potential at the exit section.

2.3. *Dimensional analysis*

Natural scales for lengths and velocities are the radius R of the capillary and the mean velocity U of the imposed flow, respectively. A convenient scale for the stresses is then the typical viscous stress $\mu U/R$. If gravity is neglected, the hydrodynamics depend on three independent parameters (e.g. Martinez & Udell 1990):

$$\alpha = a/R\,, \quad \lambda = \bar{\mu}/\mu\,, \quad Ca = \mu U/\gamma, \tag{2.19}$$

which respectively are the size of the drop relative to the capillary radius, the viscosity ratio and the capillary number, which compares viscous stresses to interfacial tension.

Section 2.2 suggests that electric current densities and streaming potentials should be scaled by $\varepsilon\zeta_c U/R^2$ and by $\varepsilon\zeta_c U/\sigma R$, respectively. Since we neglect electrohydrodynamic phenomena and there is no ζ-potential on the drop surface, the electrokinetics bring no additional parameter and depend solely on (α, λ, Ca) after non-dimensionalization.

Unless otherwise stated, an asterisk will hereafter denote a dimensionless quantity, according to the scaling proposed above and summarized in table 1. The non-dimensional pressure difference required to drive the flow along the capillary is therefore

$$\Delta p^* = \frac{R}{\mu U}\,(p_{in} - p_{out})\,, \tag{2.20}$$

and the non-dimensional streaming potential between the ends of the capillary is

$$\Delta\Phi^* = \frac{\sigma R}{\varepsilon\zeta_c U}\,(\Phi_{in} - \Phi_{out})\,. \tag{2.21}$$

https://doi.org/10.1017/S002211200999156X Published online by Cambridge University Press

In the absence of any drop, we see from (2.8) that the dimensionless pressure difference and streaming potential between the ends of a capillary of length L_w are

$$\Delta p_0^* = \Delta \Phi_0^* = 8 L_w^*. \tag{2.22}$$

The presence of the drop creates disturbances $\Delta p_a = \Delta p - \Delta p_0$ and $\Delta \Phi_a = \Delta \Phi - \Delta \Phi_0$, both of which are independent of L_w. Consequently, the difference

$$\Delta \Phi^* - \Delta p^* = \Delta \Phi_a^* - \Delta p_a^* \tag{2.23}$$

is also independent of L_w^*: we shall see later that this may be a useful experimental measurement of the change in streaming potential due to the drop, over and above that which might be expected from the change in pressure. Conversely, the apparent coupling parameter $K = \sigma \Delta \Phi / \Delta p$ is always a function of the dimensionless capillary length L_w^*; it can be computed from the perturbations Δp_a and $\Delta \Phi_a$ through

$$\frac{\mu}{\varepsilon \zeta_c} K = \frac{\Delta \Phi^*}{\Delta p^*} = 1 + \frac{\Delta \Phi^* - \Delta p^*}{\Delta p^*} = 1 + \frac{\Delta \Phi_a^* - \Delta p_a^*}{8 L_w^* + \Delta p_a^*}. \tag{2.24}$$

3. Numerical method

We consider axisymmetric configurations only. The surface integrals in (2.18) are analytically calculated in the azimuthal direction φ, using

$$\int_0^{2\pi} \frac{\mathrm{d}\varphi}{\hat{r}} = I_{01}\,, \qquad \int_0^{2\pi} \frac{\hat{\boldsymbol{r}} \cdot \boldsymbol{n}}{\hat{r}^3}\, \mathrm{d}\varphi = (\hat{r}_x n_x - y_r n_r)\, I_{30} + x_r n_r\, I_{31}, \tag{3.1}$$

with the same notations as in (2.18), and where the integrals

$$I_{mn} = \int_0^{2\pi} \frac{\cos^n \varphi}{\hat{r}^m}\, \mathrm{d}\varphi \tag{3.2}$$

can be expressed in terms of complete elliptic integral of the first and second kinds and estimated accurately by converging series. Consequently, surface integrals reduce to line integrals along the profile of the different boundaries, and only these profiles need be discretized.

The drop profile is divided into N elements defining $N+1$ nodes $(\boldsymbol{x}^0, \ldots, \boldsymbol{x}^N)$, where the two extreme nodes lie on the axis of revolution. Between two neighbouring nodes, the interface is interpolated with a cubic B-spline:

$$\boldsymbol{x}(\xi, t) = \sum_{k=-1}^{N+1} \check{\boldsymbol{x}}_k(t)\, B_k(\xi), \tag{3.3}$$

where the B_k are piecewise cubic polynomials and $\check{\boldsymbol{x}}_k$ are the spline coefficients associated with $\boldsymbol{x}$ at time t. The parameter ξ runs from 0 to 1, such that $\xi = 0$ and $\xi = 1$ correspond to the nodes $\boldsymbol{x}^0$ and $\boldsymbol{x}^N$, respectively. For each scalar variable, the spline representation (3.3) requires $N+3$ spline coefficients and two boundary conditions imposed on the axis of revolution. For a variable that vanishes on the axis owing to the axisymmetry of the problem (such as the radial component of any vector field), we impose that the second derivative with respect to ξ should be zero at $\boldsymbol{x}^0$ and $\boldsymbol{x}^N$. Otherwise, we require the first derivative to be zero. In particular, the latter condition applies to the electric potential Φ at the drop tips.

The capillary wall is discretized in a similar fashion into N_w elements, with the two extreme wall nodes $\boldsymbol{x}_w^0$ and $\boldsymbol{x}_w^{N_w}$ located respectively on the entrance and exit

https://doi.org/10.1017/S002211200999156X Published online by Cambridge University Press

sections, where boundary conditions are imposed, as discussed below. These sections are located at a distance $x = \pm L_w/2$ from the drop centre of mass, and the tube has a total length $L_w = O(10\,R)$. Note that since N_w is *a priori* different from N, a separate set of $N_w + 3$ basis functions $B_k^w(\xi)$ must be calculated.

At any time t, the flow has been determined numerically by a boundary integral method, which gives the drop interfacial velocity $\boldsymbol{u}$ and the wall shear stress $\boldsymbol{f}^w$: further details of the hydrodynamic computation are given by Lac & Sherwood (2009). To solve the electrokinetic problem (§ 2.2), only the wall shear stress is needed, since it determines the streaming current through (2.5) and (2.17). In the spline coefficient space, the integral equation (2.18) yields a linear system of size $(N+3)+(N_w+3)$, which we solve using the open-source library Lapack. This system is built with $(N+1)+(N_w-1)$ equations provided by (2.18) at the nodes $\boldsymbol{x}^j$ and $\boldsymbol{x}_w^j$ (excluding the two extreme wall nodes), together with five boundary conditions:

$$\begin{aligned} &\text{at the drop tips,} \quad \frac{\partial \Phi}{\partial r} = 0; \\ &\text{for } \boldsymbol{x} \in \mathscr{S}_w \cap \mathscr{S}_{in}, \quad \Phi = \Phi_{in} = 0, \quad \frac{\partial^2 \Phi}{\partial x^2} = 0; \\ &\text{for } \boldsymbol{x} \in \mathscr{S}_w \cap \mathscr{S}_{out}, \quad \frac{\partial^2 \Phi}{\partial x^2} = 0. \end{aligned} \tag{3.4}$$

The missing equation is given by (2.18) for $\boldsymbol{x} \in \mathscr{S}_{in}$, placed on the axis for convenience.

4. Asymptotic results for small drops and long slender drops

4.1. *A small drop on the centreline of the capillary*

We first consider the limit of a droplet of radius $a = \alpha R \ll R$ located on the centreline of the capillary. For such small drops, dimensionless capillary forces scale as $(\alpha\, Ca)^{-1}$; i.e. the drop deformability is determined by both the dimensionless drop size and the capillary number (unlike large drops, for which the surface curvature scales like R^{-1} rather than a^{-1} when $a \geqslant R$). Therefore, a sufficiently small drop will remain spherical, even if the capillary number is large.

For an asymptotically small spherical droplet, the pressure disturbance has been derived by Brenner (1971):

$$\Delta p_{\mathrm{a}}^* = \frac{\Delta p_{\mathrm{a}}}{\mu U/R} = \frac{16}{27}\frac{(2+9\lambda)^2 - 40}{(1+\lambda)(2+3\lambda)}\,\alpha^5 + O(\alpha^{10}). \tag{4.1}$$

The presence of the drop modifies the streaming potential in two ways: (*a*) the stress at the walls of the capillary is changed, thereby changing the current of convected ions, and (*b*) the electrical resistance of the fluid-filled capillary is modified. Sherwood (2009) showed that in the absence of surface conductivity, the perturbation to the streaming potential caused by the change in stress at the capillary wall is

$$\Delta \Phi_{\mathrm{a}}^* = \frac{\sigma R}{\varepsilon \zeta_c U}\,\Delta \Phi_{\mathrm{a}} \sim \alpha^5. \tag{4.2}$$

However, the reduction of conductance caused by the presence of the insulating drop leads to a non-dimensional change in potential

$$\Delta \Phi_{\mathrm{a}}^* = 16\,\alpha^3, \tag{4.3}$$

which is $O(\alpha^{-2})$ larger than the change in potential (4.2) due to stresses acting on the wall in the limit $\alpha \ll 1$. Since the additional pressure drop (4.1) decays much

https://doi.org/10.1017/S002211200999156X Published online by Cambridge University Press

faster with α than the additional streaming potential (4.3), the difference $\Delta\Phi_a^* - \Delta p_a^*$ behaves as $\Delta\Phi_a^*$ for $\alpha \ll 1$.

4.2. *Asymptotic analysis for a long slender drop in a capillary*

We consider a laminar annular flow of two liquids driven by a pressure gradient G in a capillary of radius R. The inner liquid, of viscosity $\lambda\mu$, occupies a cylinder of radius $R\delta < R$, and the outer liquid, of viscosity μ, occupies the annular film of thickness $h = (1-\delta)R$. Continuity of the fluid velocity $\boldsymbol{u}$ and of the tangential stress across the interface yields

$$\boldsymbol{u}(\boldsymbol{x}) = \begin{cases} \dfrac{G}{4\mu}(r^2 - R^2)\,\boldsymbol{e}_x, & R\delta \leqslant r \leqslant R, \\ \dfrac{G}{4\lambda\mu}\{r^2 + (\lambda-1)\delta^2 R^2 - \lambda R^2\}\,\boldsymbol{e}_x, & 0 \leqslant r \leqslant R\delta. \end{cases} \tag{4.4}$$

The total volumetric flow rate through a tube section is

$$Q = 2\pi \int_0^R \boldsymbol{u}\cdot\boldsymbol{e}_x\, r\,\mathrm{d}r = -\frac{\pi G R^4}{8\mu}\{1 + (\lambda^{-1} - 1)\delta^4\}, \tag{4.5}$$

and if we define the mean velocity U such that $Q = \pi R^2 U$, the pressure gradient is

$$G = -\frac{8\mu U}{R^2}\{1 + (\lambda^{-1} - 1)\delta^4\}^{-1}, \tag{4.6}$$

rather than $G_0 = -8\mu U/R^2$ in the absence of any drop. If the inner cylinder represents a long but finite drop moving with velocity V, then

$$\pi(R\delta)^2 V = 2\pi \int_0^{R\delta} \boldsymbol{u}\cdot\boldsymbol{e}_x\, r\,\mathrm{d}r = \frac{\pi G R^4}{8\mu}\left(2\delta^4 - 2\delta^2 - \delta^4\lambda^{-1}\right), \tag{4.7}$$

so that

$$\frac{V}{U} = -\frac{GR^2}{8\mu U}\{2 + (\lambda^{-1} - 2)\,\delta^2\} = \frac{2\lambda + (1-2\lambda)\,\delta^2}{\lambda + (1-\lambda)\,\delta^4}. \tag{4.8}$$

If the drop shape is approximated by a cylinder with two hemispherical caps of radius $R\delta$, the length l of the cylindrical part is given by

$$\frac{l}{R} \approx \frac{4}{3}(\alpha^3 - \delta^3)\,\delta^{-2}. \tag{4.9}$$

The change in pressure along the cylindrical part of the drop is Gl. There will be additional pressure losses due to the end-caps, but when $\delta \ll 1$ these are expected to scale as δ^5 according to (4.1) and can be neglected. The additional pressure Δp_a caused by the presence of the drop is therefore essentially due to the cylindrical part of the drop, i.e.

$$\Delta p_a^* = \frac{\Delta p_a}{\mu U/R} \approx \frac{(G_0 - G)\,l}{\mu U/R} \approx -\frac{32}{3}\,\frac{(1-\lambda)\,\delta^2}{\lambda + (1-\lambda)\,\delta^4}\,(\alpha^3 - \delta^3). \tag{4.10}$$

Along the length of the drop, the streaming current (2.5) generated at the capillary wall must be balanced by conduction through the fluid annulus of area $\pi(1-\delta^2)R^2$. The streaming potential gradient in the annulus is therefore

$$\frac{\partial\Phi}{\partial x} = \frac{\varepsilon\zeta_c}{\mu\sigma}\,\frac{G}{1-\delta^2}, \qquad G \equiv \frac{\partial p}{\partial x}. \tag{4.11}$$

https://doi.org/10.1017/S0022112009991566X Published online by Cambridge University Press

The disturbance in streaming potential due to the drop cylindrical part, after (2.8) and (4.11), is thus

$$\Delta\Phi_{\mathrm{a}}^{(cyl)} \approx \frac{\varepsilon\zeta_c}{\sigma\mu}\left(G_0 - \frac{G}{1-\delta^2}\right) l \tag{4.12a}$$

$$\approx \frac{32}{3}\,\frac{\lambda-(1-\lambda)(1-\delta^2)\,\delta^2}{(1-\delta^2)[\,\lambda+(1-\lambda)\,\delta^4]}\,\frac{\varepsilon\zeta_c U}{\sigma R}\,(\alpha^3-\delta^3), \tag{4.12b}$$

and (4.12*b*) indicates the possibility that $\Delta\Phi_{\mathrm{a}}^{*(cyl)} < 0$ if $\lambda < 1/5$.

The presence of the end-caps causes only a small change in the hydraulic resistance of the capillary but makes a much larger change in the electrical resistance, which, by (4.3), may be expected to be $O(\delta^3)$ when $\delta \ll 1$. There is much to be said for estimating the streaming potential due to the drop in terms of a drop length $L^* = (4/3)\alpha^3\delta^{-2}$, rather than in terms of the cylindrical length l^* defined by (4.9). However, use of L^* would lead to poorer estimates for the pressure drop caused by the drop and merely hides our ignorance of the streaming potential correction due to the end-caps. To proceed further, we note from (4.12) that when $\delta \ll 1$ the leading-order contribution to $\Delta\Phi_{\mathrm{a}}$ is due to the reduced electrical conductance of the capillary caused by the presence of the insulating drop. The cylindrical portion of the drop, when $\delta \ll 1$, contributes a change $\Delta\Phi_{\mathrm{a}}^{(cyl)} \sim -G_0\, l\,\delta^2(\varepsilon\zeta_c/\sigma\mu)$, proportional to the volume $\pi\delta^2 R^2\, l$ of the cylinder. We therefore base our estimate of the contribution of the end-caps on their volume and obtain

$$\begin{aligned}\Delta\Phi_{\mathrm{a}}^{*} &\approx \frac{\sigma R}{\varepsilon\zeta_c U}\,\Delta\Phi_{\mathrm{a}}^{(cyl)} + \frac{32}{3}\,\delta^3 \\ &\approx \frac{32}{3}\,\frac{\lambda-(1-\lambda)(1-\delta^2)\,\delta^2}{(1-\delta^2)[\,\lambda+(1-\lambda)\,\delta^4]}\,(\alpha^3-\delta^3) + \frac{32}{3}\,\delta^3.\end{aligned} \tag{4.13}$$

As discussed in § 2.3, a natural quantity to consider is the difference between the dimensionless changes in streaming potential and pressure, i.e.

$$\left.\begin{aligned}\Delta\Phi_{\mathrm{a}}^{*} - \Delta p_{\mathrm{a}}^{*} &\approx 8\,\frac{G}{G_0}\,\frac{\delta^2}{1-\delta^2}\,\frac{l}{R} + \frac{32}{3}\,\delta^3 \\ &\approx \frac{32}{3}\,\frac{\alpha^3-\delta^3}{(1-\delta^2)[1+(\lambda^{-1}-1)\,\delta^4]} + \frac{32}{3}\,\delta^3.\end{aligned}\right\} \tag{4.14}$$

Lac & Sherwood (2009) found that when $Ca \gg 1$ and $\lambda \geqslant 1/2$ the dimensionless cylindrical radius δ of the drop behaves as

$$\delta \sim (2-\lambda^{-1})^{-1/3}\,Ca^{-1/3}, \quad \lambda > 1/2, \tag{4.15a}$$

$$\delta \sim Ca^{-1/5}, \quad \lambda = 1/2, \tag{4.15b}$$

and the additional pressure drop (4.10) as

$$\Delta p_{\mathrm{a}}^{*} \sim \alpha^3\,(1-\lambda^{-1})(2-\lambda^{-1})^{-2/3}\,Ca^{-2/3}, \quad \lambda > 1/2,\ \lambda \neq 1, \tag{4.16a}$$

$$\Delta p_{\mathrm{a}}^{*} \sim -\alpha^3\,Ca^{-2/5}, \quad \lambda = 1/2, \tag{4.16b}$$

$$\Delta p_{\mathrm{a}}^{*} \sim\ Ca^{-5/3}, \quad \lambda = 1. \tag{4.16c}$$

When $\lambda = 1$ the drop viscosity is equal to that of the surrounding fluid, and the long, cylindrical portion of the drop has no effect upon the pressure drop, which is due only to the ends of the drop. The special case $\lambda = 1/2$ is more unexpected. Drops of viscosity $\lambda \geqslant 1/2$ always travel more slowly than the undisturbed centreline velocity

https://doi.org/10.1017/S002211200999156X Published online by Cambridge University Press

	$\lambda > 1/2, \quad \lambda \neq 1$	$\lambda = 1/2$	$\lambda = 1$
Δp_a^*	$\sim \alpha^3 (1-\lambda^{-1})(2-\lambda^{-1})^{-2/3} Ca^{-2/3}$	$\sim -\alpha^3 Ca^{-2/5}$	$\sim Ca^{-5/3}$
$\Delta \Phi_a^* - \frac{32}{3}\alpha^3$	$\sim \alpha^3 (2-\lambda^{-1})^{1/3} Ca^{-2/3}$	$\sim \alpha^3 Ca^{-6/5}$	$\sim \alpha^3 Ca^{-2/3}$
$\Delta \Phi_a^* - \Delta p_a^* - \frac{32}{3}\alpha^3$	$\sim \alpha^3 (2-\lambda^{-1})^{-2/3} Ca^{-2/3}$	$\sim \alpha^3 Ca^{-2/5}$	$\sim \alpha^3 Ca^{-2/3}$

TABLE 2. Asymptotic behaviour of the pressure and streaming potential disturbances due to an elongated drop of size $a = \alpha R$ at high Ca and for $\lambda \geqslant 1/2$.

in the capillary; i.e. the drop velocity V is lower than $2U$. If $\lambda < 1/2$, V exceeds $2U$ at sufficiently high Ca, and as a result the streamlines at the end of the drop take quite a different form (Lac & Sherwood, 2009).

As $\delta \to 0$, the effect of the drop on the pressure gradient (4.6) decreases as δ^4. Consequently, even though the length of the drop increases as δ^{-2}, the additional pressure drop Δp_a decays to zero for $\lambda \geqslant 1/2$. However, the electrical resistance per unit length of the capillary is perturbed by an amount $O(\delta^2)$, which when combined with the increasing drop length $O(\delta^{-2})$ leads to a finite change in total resistance and streaming potential. We deduce from (4.13) that when $\lambda \geqslant 1/2$ the change in streaming potential $\Delta \Phi_a^*$ tends to the constant value $(32/3)\alpha^3$ depending on the drop volume, at a rate

$$\Delta \Phi_a^* - \frac{32}{3}\alpha^3 \sim \frac{32}{3}(2-\lambda^{-1})(\alpha^3 - \delta^3)\delta^2 + \frac{32}{3}(\lambda^{-2}-1)\alpha^3\delta^6 + O(\delta^8), \quad (4.17a)$$

$$\Delta \Phi_a^* - \frac{32}{3}\alpha^3 \sim \alpha^3 (2-\lambda^{-1})^{1/3} Ca^{-2/3}, \quad \lambda > 1/2, \quad (4.17b)$$

$$\Delta \Phi_a^* - \frac{32}{3}\alpha^3 \sim \alpha^3 Ca^{-6/5}, \quad \lambda = 1/2, \quad (4.17c)$$

where we note that (4.17c) relies on our choice $(32/3)\delta^3$ for the end-cap correction in (4.13): any other choice would lead to a contribution $O(Ca^{-3/5})$, far removed from the numerical results to be presented in § 5.3. However, these numerical results also suggest that the end-cap correction should contain additional terms of higher order than δ^3, which ultimately dominate the $\alpha^3\delta^6$ contribution corresponding to (4.17c). The unknown contribution of the end-caps does not affect the leading-order behaviour of the difference $\Delta \Phi_a^* - \Delta p_a^*$ when $\delta \to 0$, and (4.14) leads to

$$\Delta \Phi_a^* - \Delta p_a^* - \frac{32}{3}\alpha^3 \sim \alpha^3 (2-\lambda^{-1})^{-2/3} Ca^{-2/3}, \quad \lambda > 1/2, \quad (4.18a)$$

$$\Delta \Phi_a^* - \Delta p_a^* - \frac{32}{3}\alpha^3 \sim \alpha^3 Ca^{-2/5}, \quad \lambda = 1/2. \quad (4.18b)$$

The asymptotic behaviours (4.16)–(4.18) obtained for $\lambda \geqslant 1/2$ are summarized in table 2. For $\lambda < 1/2$ the numerical computations of Lac & Sherwood (2009) indicate that at large capillary numbers, the cylindrical radius δ of the drop tends to a limit that was found empirically to be

$$\delta_\infty = \sqrt{\frac{2}{5}\frac{1-2\lambda}{1-\lambda}}, \quad (4.19)$$

leading to limit values for Δp_a^* and $\Delta \Phi_a^*$ through (4.10) and (4.13).

https://doi.org/10.1017/S002211200999156X Published online by Cambridge University Press

5. Arbitrary drop size

We now investigate numerically the effect of the parameters α, Ca and λ on the additional pressure drop and streaming potential. The influence of the viscosity contrast is investigated by comparing the results obtained for three values of λ. We choose $\lambda = 0.1$ and 10 to address the cases of low- and high-viscosity drops, respectively, and $\lambda = 1$ to highlight the effect of size and capillarity, independently of viscous effects.

5.1. *Effect of drop size*

The streaming potential perturbation $\Delta\Phi_a$ is shown in figure 3 as a function of the drop size a for different viscosity ratios and capillary numbers. As discussed in § 4.1, the streaming potential disturbance is caused (a) by the change in electrical resistance of the capillary owing to the presence of the insulating drop and (b) by the change in the convective current due to the non-uniform shear rate created by the motion of the viscous drop (i.e. a hydrodynamic effect). For small spherical droplets, the dominant effect comes from the change of electrical resistance (§ 4.1). The resulting potential perturbation is therefore independent of λ and always positive; we find a very good agreement between our numerical results and prediction (4.3) for $\alpha = O(0.1)$. As the drop size increases, an increasingly long viscous film eventually appears between the deformed drop and the capillary wall. The wall shear rate (and hence the convective electric current) in the film region depends upon the viscosity contrast between the drop and the wetting phase. If $\lambda < 1$, the streaming current induced by the drop in the film region is lower than that of the single-phase flow, leading to a decreasing perturbation $\Delta\Phi_a$ as the drop size increases, and vice versa for $\lambda > 1$. For very large drops, this film regime is dominant, since the effect of the drop ends may be neglected. It yields $\Delta\Phi_a^* \sim \alpha^3$ (cf. (4.17)) as can be seen in figures 3(b) and 3(c). For low-viscosity drops, the competition, at fixed capillary number, between viscous effects (decreasing the streaming potential) and the additional resistivity effect (enhancing the streaming potential) leads to a maximum perturbation $\Delta\Phi_a$ as the drop volume varies (figure 3a). When $\lambda \geqslant 1$, on the other hand, $\Delta\Phi_a^*$ monotonically increases with α (figures 3b and 3c). This suggests gas bubbles and viscous oil droplets in water-wet rocks should generate very different streaming potential responses.

Figure 4 shows the perturbation $\Delta\Phi_a^* - \Delta p_a^*$ as a function of the drop size, for different viscosity ratios. We observe that this quantity is always positive, which enables us to display the effect of λ more clearly, since all the data can be shown on the same logarithmic scale. The thick dashed lines in figures 3 and 4 show, for $\lambda = 1, 10$, the slope α^3 predicted by (4.17) and (4.18) for long drops when $\lambda \geqslant 0.5$. For given (λ, Ca) any increase in the volume of the drop merely lengthens the cylindrical portion of the drop of radius δ (which remains unchanged), as discussed by Lac & Sherwood (2009). The α^3 dependence of $\Delta\Phi_a^*$ and $\Delta\Phi_a^* - \Delta p_a^*$ is therefore expected for all Ca as long as the drop is sufficiently long for end corrections to be negligible, as predicted by (4.13) and (4.14). Although the numerical prefactor in expression (4.15) for δ is unknown, we know that $0 < \delta < 1$, and so, by (4.13) and (4.14), the disturbances $\Delta\Phi_a^*$ and $\Delta\Phi_a^* - \Delta p_a^*$ approach $(32/3)\alpha^3$ from above as Ca increases, as seen in figures 3 and 4.

5.2. *Spherical drops: $Ca = 0$*

If $\alpha < 1$, the drop is sufficiently small such that it can fit undeformed within the capillary, and we can therefore investigate the case of an undeformed spherical drop ($Ca = 0$), for which analytic results are available when the gap $1 - \alpha$ between the

https://doi.org/10.1017/S002211200999156X Published online by Cambridge University Press

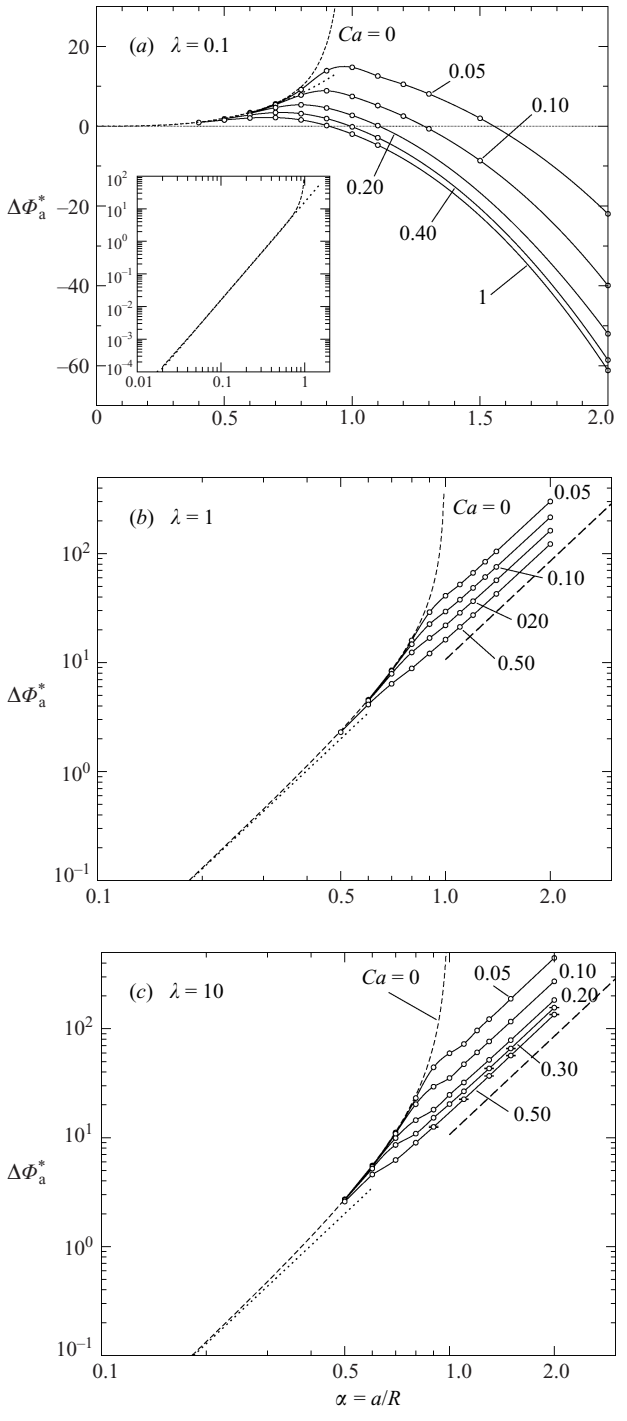


FIGURE 3. Effect of drop size on $\Delta\Phi_a^*$ for $\lambda = 0.1, 1, 10$ and different capillary numbers: dotted line, asymptotic prediction (4.3) for small spherical drops; thick dashed line in (*b*) and (*c*), asymptote $(32/3)\alpha^3$ predicted by (4.17) for long drops at high *Ca* and $\lambda \geqslant 1/2$.

https://doi.org/10.1017/S002211200999156X Published online by Cambridge University Press

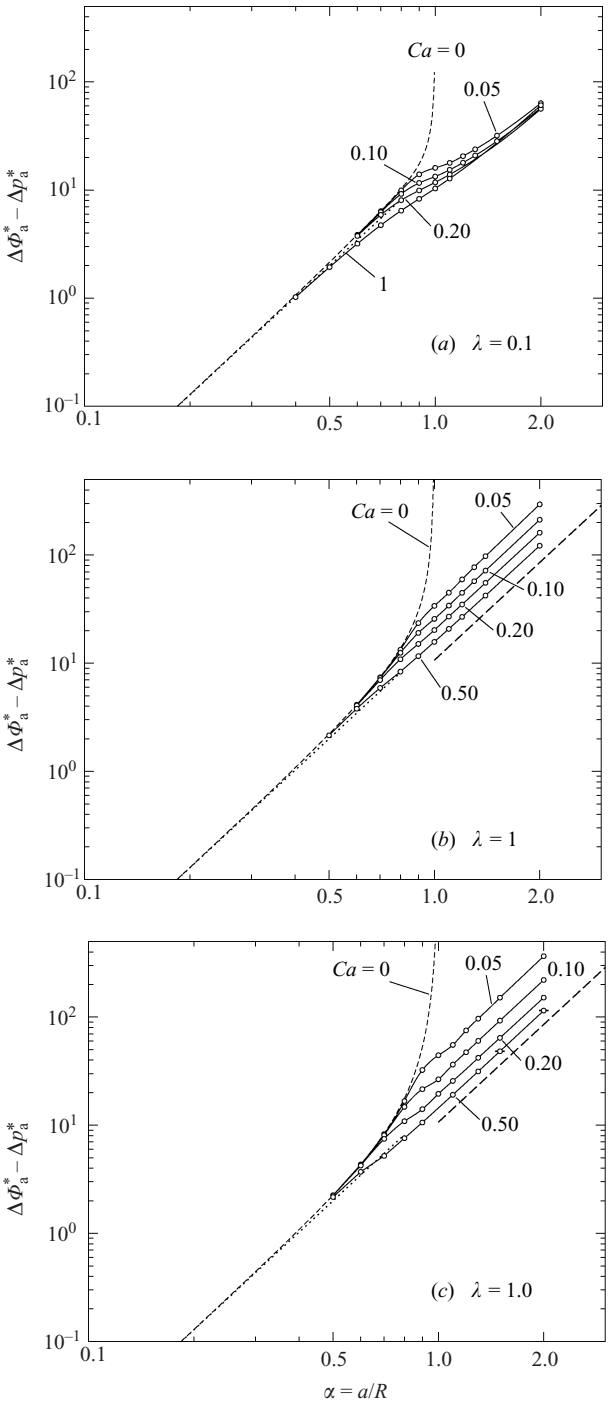


FIGURE 4. Same as figure 3 for $\Delta\Phi_a^* - \Delta p_a^*$: dotted line, asymptotic prediction (4.3) for small spherical drops; thick dashed line in (*b*) and (*c*), asymptote $(32/3)\alpha^3$ predicted by (4.18) for long drops at high *Ca* and $\lambda \geqslant 1/2$.

https://doi.org/10.1017/S002211200999156X Published online by Cambridge University Press

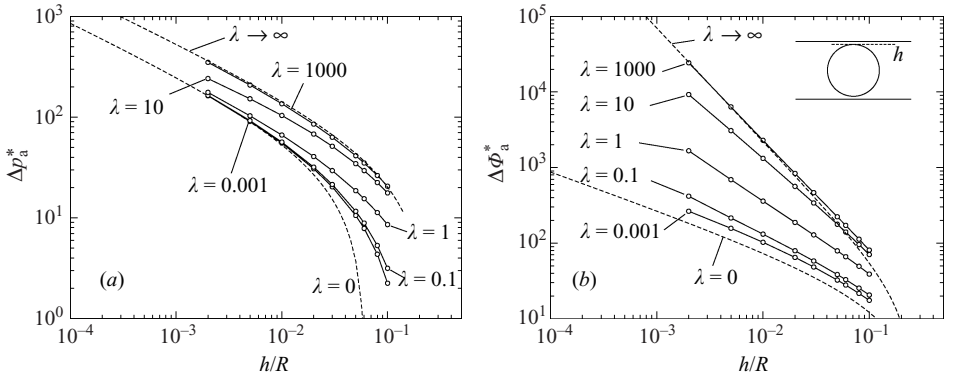


FIGURE 5. Additional pressure drop and streaming potential generated by a closely fitting spherical drop in the capillary at $Ca = 0$: (*a*) Δp_a^* and (*b*) $\Delta \Phi_a^*$ versus gap width $h = R - a$ for a range of viscosity ratios. The dashed lines denote asymptotic predictions for $\lambda = 0$ and $\lambda \to \infty$ given by (5.1) (with -36 added to the right-hand side) and (5.2) (with -16 added).

drop and the capillary is small. A somewhat different numerical scheme is required for the hydrodynamical computation, as discussed by Lac & Sherwood (2009), but the computation of the streaming potential is unaffected. Figure 5 shows the additional pressure drop and streaming potential as functions of the gap width $h/R = 1 - \alpha$ between the drop and the wall, for $0.9 \leqslant \alpha < 1$ and over a wide range of viscosity ratios. In the limit $h/R \ll 1$, lubrication analysis (Hochmuth & Sutera 1970; Bungay & Brenner 1973; Sherwood 2007) predicts the additional pressure drop:

$$\Delta p_a^* = 2\pi \left(\frac{h}{2R}\right)^{-1/2}, \quad \lambda = 0\,; \tag{5.1a}$$

$$\Delta p_a^* = 4\pi \left(\frac{h}{2R}\right)^{-1/2}, \quad \lambda \to \infty. \tag{5.1b}$$

The next term in the expansion for Δp_a^* is presumably a constant, and by adding -36 to the right-hand sides of (5.1*a*) and (5.1*b*) we get good agreement with the full numerical results for Δp_a^*, as seen in figure 5(*a*). This added constant is comparable to the value -31.5 proposed by Hochmuth & Sutera (1970) for the case of a rigid sphere. The corresponding streaming potentials were studied by Sherwood (2007), who found

$$\Delta \Phi_a^* = 2\pi \left(\frac{h}{2R}\right)^{-1/2}, \quad \lambda = 0\,, \tag{5.2a}$$

$$\Delta \Phi_a^* = \frac{\pi}{4} \left(\frac{h}{2R}\right)^{-3/2}, \quad \lambda \to \infty. \tag{5.2b}$$

The next term in expansion (5.2*a*) is presumably a constant. We add -16 to the right-hand sides of both (5.2*a*) and (5.2*b*), after which figure 5(*b*) shows good agreement between (5.2*b*) and full numerical results for $\lambda > 100$. This constant -16, chosen arbitrarily to improve the agreement with the full numerical results, corresponds to the streaming potential across a length $2R$ of capillary in the absence of any spherical particle. As λ decreases, so does the streaming potential, until no appreciable difference is observed between $\lambda = 0.01$ (not shown for clarity) and $\lambda = 0.001$. However, there is an unresolved discrepancy between the computed $\Delta \Phi_a^*$ and (5.2*a*) in the range of h/R

https://doi.org/10.1017/S002211200999156X Published online by Cambridge University Press

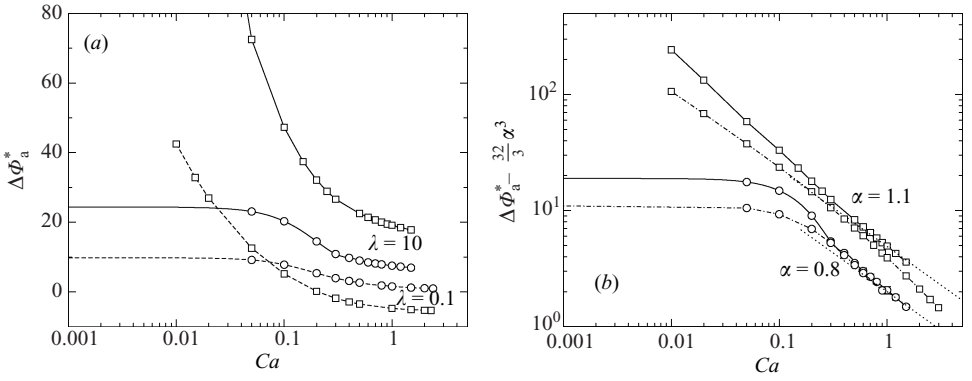


FIGURE 6. (*a*) Additional streaming potential $\Delta\Phi_a^*$ versus Ca: ○, $\alpha = 0.8$; □, $\alpha = 1.1$. (*b*) As for (*a*) but showing how $\Delta\Phi_a^*$ approaches the value $(32/3)\alpha^3$ predicted for $\lambda \geqslant 0.5$ as Ca increases: dotted lines, $\sim Ca^{-2/3}$; dashed, dot-dashed, solid lines, $\lambda = 0.1, 1, 10$, respectively.

shown in figure 5. This may in part be due to the fact that for the inviscid bubble the streaming potential increases only as $(h/R)^{-1/2}$ as $h \to 0$. The effect of the thin film dominates that of the rear and front caps only when $h \ll R$. Unfortunately, we have not been able to simulate dimensionless gaps smaller than 0.002 owing to instabilities arising in the numerical method.

5.3. *Effect of the capillary number*

We now investigate the effect of the capillary number at fixed drop volume and viscosity ratio. Figure 6 shows the evolution of the additional streaming potential $\Delta\Phi_a^*$ under increasing flow strength. Since the drop is insulating, its presence in the capillary increases the electrical resistance of the tube, which tends to increase the streaming potential. On the other hand, the streaming current depends on the wall shear rate. As a result, the actual value (and sign) of $\Delta\Phi_a^*$ is a function of (α, λ, Ca). When $\lambda > 1$, the streaming current is always enhanced by the motion of the drop, and $\Delta\Phi_a^*$ is positive for all drop volumes, for all Ca (figure 6*a*, $\lambda = 10$). At sufficiently small capillary number, the enhanced electrical resistivity and capillary effects due to the drop ends dominate viscous effects, and $\Delta\Phi_a^*$ is positive even when $\lambda < 1/5$. The effect of low viscosity is therefore visible only for sufficiently large drops and capillary numbers (figure 6*a*, $\lambda = 0.1$, $\alpha = 1.1$). Figure 6(*b*) shows how the additional streaming potential reaches the asymptotic value $(32/3)\alpha^3$ predicted for a viscous drop ($\lambda \geqslant 0.5$) at large capillary numbers (§4.2). Our numerical results follow the predicted behaviour $\sim Ca^{-2/3}$ for $\lambda = 10$, whereas the agreement is poorer for $\lambda = 1$, for which $\Delta\Phi_a^*$ decays faster than predicted. In this case, the absence of viscosity contrast leaves the wall shear rate (and therefore the streaming current) equal to that for single-phase flow. The end-caps therefore play a more important role than usual unless the drop is exceedingly long.

Figure 7 is the counterpart of figure 6 for the difference $\Delta\Phi_a^* - \Delta p_a^*$. We see that this difference becomes smaller for $\lambda = 10$ than for $\lambda = 1$ at sufficiently high Ca, as predicted by (4.18*a*). However, the predicted $\sim Ca^{-2/3}$ decay at high capillary numbers is poorly captured by our numerical results. For the particular viscosity ratio $\lambda = 1/2$ (figure 8), the difference $\Delta\Phi_a^* - \Delta p_a^*$ at large Ca is dominated by the pressure drop, which decays more slowly than the streaming potential as Ca increases (see table 2). The behaviour of the streaming potential $\Delta\Phi_a^*$ depends upon unknown corrections

https://doi.org/10.1017/S0022112009991566 Published online by Cambridge University Press

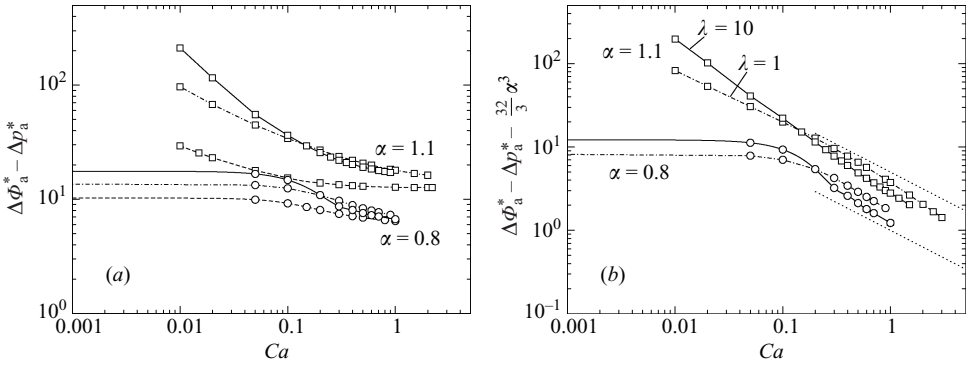


FIGURE 7. Same as figure 6 for the perturbation $\Delta\Phi_a^* - \Delta p_a^*$.

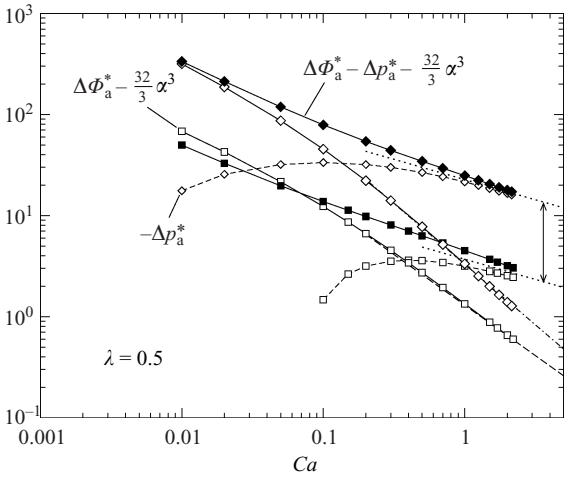


FIGURE 8. Drops with $\lambda = 0.5$: □, $\alpha = 1.1$; ◇, $\alpha = 2$. The filled symbols show how $\Delta\Phi_a^* - \Delta p_a^*$ approaches the value $(32/3)\alpha^3$ as Ca increases. The open symbols and solid lines denote $\Delta\Phi_a^* - (32/3)\alpha^3$; the dashed lines denote $-\Delta p_a^*$; the dotted, dot-dashed and long dashed lines denote $\sim Ca^{-2/5}$, $\sim Ca^{-6/5}$ and $\sim Ca^{-1}$, respectively. The arrow denotes a multiplying factor of $(2/1.1)^{\pm 3}$.

for the end-caps, and the prediction of (4.17*c*) for the rate at which $\Delta\Phi_a^*$ approaches $(32/3)\alpha^3$ seems to correspond to the numerical results for the longer of the two drops shown in figure 8 ($\alpha = 2$). However, when $\alpha = 1.1$ the rate of decay of $\Delta\Phi_a^* - (32/3)\alpha^3$ is slower than $Ca^{-6/5}$, and the line $\sim Ca^{-1}$ shown in the figure corresponds to an additional end-cap correction $O(\delta^5)$ in (4.13) and in (4.17*a*). Such a correction would ultimately dominate the $\alpha^3 Ca^{-6/5}$ prediction of (4.17*c*), and this would seem to have already occurred for the smaller of the two drops. A thorough analysis of the end-cap contribution would be required to confirm this hypothesis.

The validity of the long slender drop approximation (§ 4.2) is investigated in figures 9 and 10, which show $\Delta\Phi_a^*$ and $\Delta\Phi_a^* - \Delta p_a^*$ as functions of the film thickness h, for $\alpha = 2$. For a given viscosity ratio, we find that the difference between the annular model and the numerical results decreases as Ca increases. This is expected, since the drop thins and elongates as Ca increases, thereby more nearly satisfying the assumptions which lead to (4.13) and (4.14). These approximations provide estimates

https://doi.org/10.1017/S002211200999156X Published online by Cambridge University Press

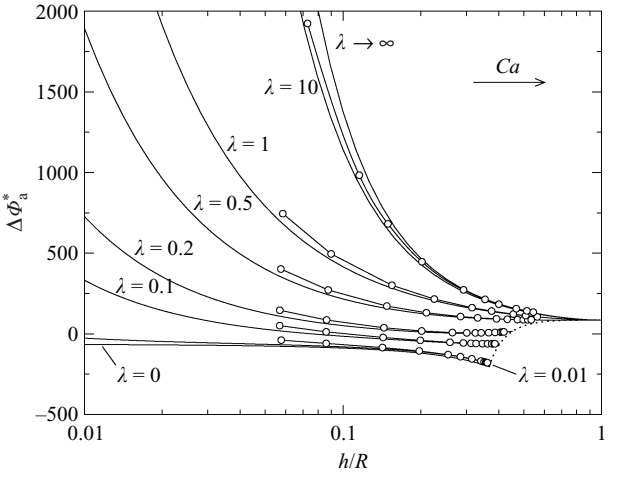


FIGURE 9. Additional streaming potential $\Delta\Phi_a^*$ versus film thickness h for very long drops ($\alpha = 2$): thin lines, long-drop approximation (4.13); ○, numerical results; dotted line, limit values (4.19) combined with (4.13) for $\lambda < 0.5$.

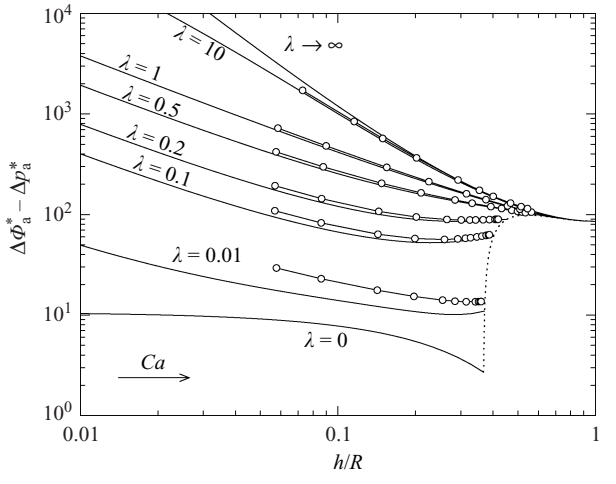


FIGURE 10. Same as figure 9 for $\Delta\Phi_a^* - \Delta p_a^*$.

of the pressure drop and streaming potential disturbances either in terms of δ or in terms of the drop velocity (easily measured experimentally), since V/U yields δ through (4.8).

We finally show in figure 11 the effect of viscosity contrast on streaming potential at $Ca = 0.05$ and for three drop sizes, $\alpha = 0.8, 1.1, 2$. We first note that $\Delta\Phi_a^*$ reaches a plateau value at large viscosity contrasts, i.e. λ or $\lambda^{-1} \gg 1$ (figure 11*a*). The rate of change of $\Delta\Phi_a^*$ with λ is greatest in the range $0.1 \leqslant \lambda \leqslant 5$, typically. The streaming potential generated by small drops is reasonably well estimated by the limit $Ca = 0$, corresponding to a spherical drop with infinite surface tension. Since sufficiently small drops are virtually undeformable, the agreement improves as α decreases below 0.8 (not shown in figure 11 for clarity). We see from figure 11 that the long-drop approximation is not valid for a drop volume corresponding to $\alpha = 1.1$ at this low

https://doi.org/10.1017/S0022112009991566X Published online by Cambridge University Press

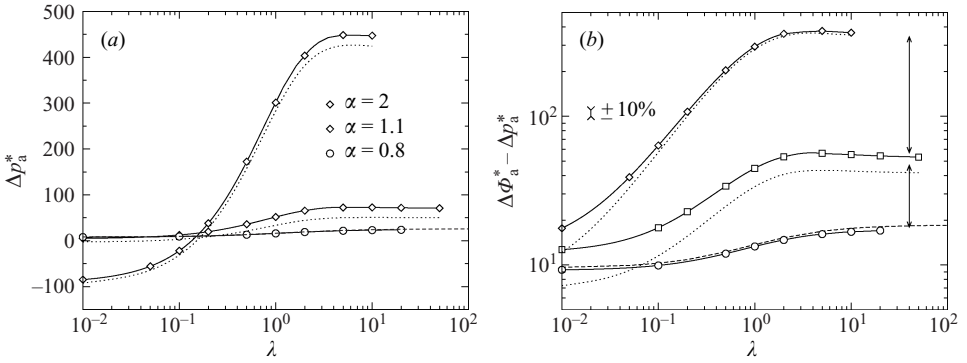


FIGURE 11. Perturbations $\Delta\Phi_a^*$ and $\Delta\Phi_a^* - \Delta p_a^*$ as a function of λ for $Ca = 0.05$ and three drop sizes: ○, $\alpha = 0.8$; □, $\alpha = 1.1$; ◇, $\alpha = 2$; dashed line, $\alpha = 0.8$, $Ca = 0$; dotted line, long-drop approximation; arrows, volume ratio factors of $(1.1/0.8)^{\pm 3}$ and $(2/1.1)^{\pm 3}$.

capillary number; for this drop size, the cylindrical part, if any, is extremely short, and so the dominating disturbance comes from the end-caps, for which we have but a poor estimate – the term $(32/3)\delta^3$ in (4.13) and (4.14). For $Ca = 0.05$ and $\alpha = 2$, we see that the long-drop approximation of $\Delta\Phi_a^*$ and $\Delta\Phi_a^* - \Delta p_a^*$ is indeed much better than when $\alpha = 1.1$. For long, high-viscosity drops, viscous effects (affecting streaming currents) and global electrical resistance increase linearly with the drop volume; hence increasing the relative drop size α rapidly increases both $\Delta\Phi_a^*$ and $\Delta\Phi_a^* - \Delta p_a^*$. This effect is weaker at low viscosity ratios because hydrodynamic and additional resistance effects compete (figure 11*b*).

6. Conclusion

The main purpose of this paper was to predict streaming potentials in capillary flow, in the presence of a drop of arbitrary size and viscosity, and thereby extend the results of Sherwood (2007), who considered only rigid or inviscid drops that fitted tightly in the capillary. The purely hydrodynamic results, of interest to a larger community than that involved in electrokinetic problems, have been presented in a separate paper (Lac & Sherwood, 2009). However, many of the results obtained here for the change in streaming potential $\Delta\Phi_a^*$ caused by the presence of the drop are closely related to equivalent results for the change in the pressure drop Δp_a^* caused by the drop.

The sign of $\Delta\Phi_a^*$ depends upon the drop viscosity, but unlike Δp_a^* the change in the sign of $\Delta\Phi_a^*$ does not occur at $\lambda = 1$. The presence of the non-conducting drop reduces the average conductivity of the capillary and tends to increase the streaming potential. However, when $\lambda < 1$ the reduced pressure gradient caused by the presence of the low-viscosity drop reduces the streaming current and hence tends to reduce the streaming potential. Competition between these two effects determines the sign of $\Delta\Phi_a^*$. A reduced streaming potential ($\Delta\Phi_a^* < 0$) is possible for a long drop if $\lambda < 1/5$ (cf. (4.12)), though we have shown in § 4.1 that the dimensionless streaming potential is always enhanced if the drop is sufficiently small (e.g. figure 3*a*).

Single-phase flow experiments typically determine the coupling coefficient of proportionality between applied pressure and measured streaming potential. The introduction of a second fluid phase usually modifies the pressure gradient required to achieve any particular flow rate, and the change in streaming potential over and

https://doi.org/10.1017/S002211200999156X Published online by Cambridge University Press

above that which might be expected solely on the basis of the change in pressure is $\Delta\Phi_a^* - \Delta p_a^*$. The computational results of § 5 become much more consistent when expressed as the difference $\Delta\Phi_a^* - \Delta p_a^*$ (which is always positive).

The hydrodynamic behaviour of the drop at large *Ca*, discussed by Lac & Sherwood (2009), directly affects the streaming potential. If $\lambda < 1/2$ the drop does not elongate indefinitely but tends towards a limiting cylindrical diameter before breaking. It is therefore natural that $\Delta\Phi_a^*$ tends to a limit. More unexpected is the behaviour for $\lambda \geqslant 1/2$, when the drop elongates indefinitely as *Ca* increases. As the interface of the drop approaches the centreline of the capillary, the change in shear rate at the capillary wall is reduced, and the main effect of the drop is to change the conductivity of the capillary. However, as the drop lengthens, its cross-section is reduced: the total change in electrical resistance, which depends on the drop volume, is unaltered. The net effect is a limiting value $(32/3)\alpha^3$ for $\Delta\Phi_a^*$, whereas the pressure disturbance vanishes.

The results presented here remain to be tested by experiment. The narrow gap between the drop and the capillary wall plays an important role, particularly at low *Ca*, and Sherwood (2008) has given estimates for the streaming potentials that might have to be measured in experiments at low *Ca*. At the higher flow rates discussed here, the streaming potentials would be larger and so more easily measured, but the percentage change in streaming potential caused by the presence of the elongated drop would be reduced (see e.g. figure 7). In other geometries (e.g. non-circular channels) the effect of *Ca* is likely to be reduced, since the continuous, wetting fluid always occupies the channel corners and the electrical conductance does not drop to zero as $Ca \to 0$.

Several simplifying assumptions have been made in order to make the problem considered here more tractable. For example, surface charge at the surface of the drop has been neglected: our understanding of charge at liquid–liquid interfaces is more limited than at a solid interface. If the surface charge is due to adsorbed surfactants, a full computation would require knowledge of the adsorption isotherm, of the proportion of surfactants that are charged and of Marangoni effects caused by changes in interfacial tension (Baygents & Saville 1991). Such details are beyond the scope of the current study. Our assumption that the drop is non-conducting is probably appropriate for an oil droplet in water but not for water in oil. Debye lengths κ^{-1} are typically of the order of nanometres in water; so our assumption that $\kappa^{-1} \ll h$ and charge clouds are thin is reasonable in water at all but the lowest capillary numbers. However, the ionic number density is much lower in very low-conductivity oils than in water, and Debye lengths would be much larger. Zeta-potentials at a solid surface are typically in the range 0–100 mV, which correspond to a non-dimensional potential $0 \leqslant |e\zeta_c/kT| < 4$. Linearization of the Poisson–Boltzmann equation governing the equilibrium electric charge cloud requires $|e\zeta_c/kT| \ll 1$, and there is scope for work to extend the results presented here to higher potentials. In particular, at high potentials electric Hartmann numbers may not be small, and the fluid velocity may be modified by the electric field. Under such circumstances it will no longer be possible to decouple the hydrodynamic part of the computation from the computation of the electric field. This decoupling was used when obtaining the results presented here and was an important simplification of the computational scheme.

Finally, we point out that the flow geometry in porous rock rarely consists of straight capillaries, and there is much to be done in more realistic geometries. In future work we hope to remove some of the simplifying assumptions listed above.

https://doi.org/10.1017/S002211200999156X Published online by Cambridge University Press

This work was partially funded by an EU Marie Curie fellowship awarded to E.L., contract IEF-041766 (EOTIP). We thank the referees of both this and the preceding hydrodynamic paper (Lac & Sherwood, 2009) for helpful comments.

REFERENCES

Antraygues, P. & Aubert, M. 1993 Self potential generated by two-phase flow in a porous medium: experimental study and volcanological applications. *J. Geophys. Res.* **98** (B12), 22273–22281.

Baygents, J. C. & Saville, D. A. 1991 Electrophoresis of drops and bubbles. *J. Chem. Soc., Faraday Trans.* **87**, 1883–1898.

Brenner, H. 1971 Pressure drop due to the motion of neutrally buoyant particles in duct flows. II. Spherical droplets and bubbles. *Indus. Engng Chem. Fundam.* **10** (4), 537–543.

Brunet, E. & Ajdari, A. 2006 Thin double layer approximation to describe streaming current fields in complex geometries: analytical framework and applications to microfluidics. *Phys. Rev.* E **73** (5), 056306.

Bungay, P. M. & Brenner, H. 1973 The motion of a closely-fitting sphere in a fluid-filled tube. *Intl J. Multiphase Flow* **1**, 25–56.

Guichet, X., Jouniaux, L. & Pozzi, J.-P. 2003 Streaming potential of a sand column in partial saturation conditions. *J. Geophys. Res.* **108** (B3), 2141.

Hochmuth, R. M. & Sutera, S. P. 1970 Spherical caps in low Reynolds number tube flow. *Chem. Engng Sci.* **25**, 593–604.

Hunter, R. J. 1981 *Zeta Potential in Colloid Science*. Academic.

Jackson, M. D. 2008 Characterization of multiphase electrokinetic coupling using a bundle of capillary tubes model. *J. Geophys. Res.* **113**, B04201.

Jackson, M. D., Saunders, J. H. & Addiego-Guevara, E. A. 2005 Development and application of new downhole technology to detect water encroachment towards intelligent wells, Paper 97063. In *Society of Petroleum Engineers Annual Technical Conference, 9–12 October 2005*, Dallas, TX.

Lac, E. & Sherwood, J. D. 2009 Motion of a drop along the centreline of a capillary in a pressure-driven flow. *J. Fluid Mech.* (in press) doi:10.1017/S0022112009991212.

Liron, N. & Shahar, R. 1978 Stokes flow due to a Stokeslet in a pipe. *J. Fluid Mech.* **86** (4), 727–744.

Martinez, M. J. & Udell, K. S. 1990 Axisymmetric creeping motion of drops through circular tubes. *J. Fluid Mech.* **210**, 565–591.

Melcher, J. R. & Taylor, G. I. 1969 Electrohydrodynamics: a review of the role of interfacial shear stresses. *Annu. Rev. Fluid Mech.* **1**, 111–146.

Morgan, F. D., Williams, E. R. & Madden, T. R. 1989 Streaming potential properties of westerly granite with applications. *J. Geophys. Res.* B **94**, 12449–12461.

Olbricht, W. L. 1996 Pore-scale prototypes of multiphase flow in porous media. *Annu. Rev. Fluid Mech.* **28**, 187–213.

Revil, A. & Cerepi, A. 2004 Streaming potentials in two-phase flow conditions. *Geophys. Res. Lett.* **31**, L11605.

Revil, A., Schwaeger, H., Cathles III, L. M. & Manhardt, P. D. 1999 Streaming potential in porous media. Part 2. Theory and application to geothermal systems. *J. Geophys. Res.* **104** (B9), 20033–20048.

Saunders, J. H., Jackson, M. D. & Pain, C. C. 2006 A new numerical model of electrokinetic potential response during hydrocarbon recovery. *Geophys. Res. Lett.* **33**, L15316.

Saunders, J. H., Jackson, M. D. & Pain, C. C. 2008 Fluid flow monitoring in oilfields using downhole measurements of electrokinetic potential. *Geophysics* **73** (5), E165–E180.

Saville, D. A. 1997 Electrohydrodynamics: the Taylor–Melcher leaky dielectric model. *Annu. Rev. Fluid Mech.* **29**, 27–64.

Sherwood, J. D. 2007 Streaming potential generated by two-phase flow in a capillary. *Phys. Fluids* **19**, 053101.

Sherwood, J. D. 2008 Streaming potential generated by a long viscous drop in a capillary. *Langmuir* **24** (18), 10011–10018.

https://doi.org/10.1017/S002211200999156X Published online by Cambridge University Press

Sherwood, J. D. 2009 Streaming potential generated by a small charged drop in Poiseuille flow. *Phys. Fluids* **21**, 013101.

Sprunt, E. S., Mercer, T. B. & Djabbarah, N. F. 1994 Streaming potential from multiphase flow. *Geophysics* **59** (5), 707–711.

Tsai, T. M. & Miksis, M. J. 1994 Dynamics of a drop in a constricted capillary tube. *J. Fluid Mech.* **274**, 197–217.

Wurmstich, B. & Morgan, F. 1994 Modeling of streaming potential responses caused by oil well pumping. *Geophysics* **59** (1), 46–56.

https://doi.org/10.1017/S002211200999156X Published online by Cambridge University Press